Asgard ESCRT-IIIs assemble into helical filaments in the presence of DNA and remodel eukaryotic membranes

Nataly Melnikov[1,2], Dikla Nachmias[1,2], Gal Halbi[3], Alexander Upcher[4], Ran Zalk[4], Ann Bernheim-Groswasser[3,4], Natalie Elia[1,2]

1 Department of Life Sciences, Ben-Gurion University of the Negev, Beer Sheva 84105, Israel

2 National Institute for Biotechnology in the Negev (NIBN), Ben-Gurion University of the Negev, Beer Sheva 84105, Israel

3 Department of Chemical Engineering, Ben-Gurion University of the Negev, Beer Sheva 84105, Israel

4 Ilse Katz Institute for Nanoscale Science and Technology, Ben Gurion University of the Negev, Beer Sheva 84105, Israel

* Corresponding author:
Natalie Elia
Phone: 972-8-6428735
Email: elianat@post.bgu.ac.il

ABSTRACT

The ESCRT machinery mediate membrane remodeling in numerous processes in cells including cell division and nuclear membrane reformation. The identification of ESCRT homologs in Asgard archaea, currently considered the closest ancestor of eukaryotes, suggests a role for ESCRTs in the membrane remodeling processes that occurred during eukaryogenesis. Yet, the function of these distant ESCRT homologs is mostly unresolved. Here we show that Asgard ESCRT-III proteins self-assemble into homo- and hetero- helical tubes, a hallmark of the eukaryotic ESCRT system. Asgard ESCRT-III tube assembly was facilitated in the presence of DNA and inhibited by DNAase. Notably, Asgard ESCRT-III filaments remodeled eukaryotic-like membrane vesicles, also in the presence of DNA, indicating an ancient role for the ESCRT complex in membrane remodeling, that may involve DNA binding. The ability of Asgard archaeal ESCRTs to remodel eukaryotic-like membranes, places them at the junction between prokaryotes and eukaryotes, substantiating a role for ESCRTs in eukaryogenesis.

INTRODUCTION

The Asgard superphyla, manifest a unique branch that, according to current evolutionary theories, is considered to be the closest prokaryotic relative of eukaryotes. All Asgard archaeal species were found to encode for Eukaryotic Signature Proteins (ESPs), that carry cellular functions that until recently were considered as exclusive to eukaryotes (1-3). Thus, Asgard proteins potentially hold the core functions of ancient eukaryotic cellular machines. Of particular interest, are ESPs with membrane remodelling capabilities, as these proteins may contribute to the establishment of cellular compartmentalization during eukaryogenesis. Indeed, Asgard archaea encode for several eukaryotic membrane remodelling machineries including the SNARE complex, BAR domains proteins and the ESCRT machinery (1, 3, 4). Among these machineries, ESCRTs are the most conserved and are encoded by all Asgard species

discovered up to date, suggesting that they carry essential functions in these unique prokaryotes (5, 6).

The ESCRT machinery constitute one of the most robust and versatile cellular apparatus for membrane constriction and fission. Proteins of the machinery are encoded by all domains of life and were shown to mediate membrane remodelling in a wide range of eukaryotic cellular membranes including plasma membrane, nuclear membrane and endocytic membranes (7, 8). Moreover, ESCRT-mediated processes span a large spectrum of length scales, from less than 100 nm for vesicle release to up to 1 µm for cell division. How the ESCRT complex mediate membrane remodelling in this large landscape of membrane sources and length scales is mostly unknown (9).

The eukaryotic ESCRT system is composed of five subfamilies, i.e. ESCRT 0-III and the AAA-ATPase VPS4. Within this complex, ESCRT-III (named CHMPs in animal cells) and VPS4 manifest the minimal unit required for driving membrane fission (9, 10). According to current models, membrane constriction and scission are mediated by polymerization of ESCRT-III proteins into helical hetero-filaments and their remodelling by VPS4 (10-14). Indeed, ESCRT-III proteins have been shown organize in helical filaments and tubes both in vitro and in cells (14-19). However, the large number of proteins within the ESCRT-III subfamily —twelve in humans and eight in yeast - have challenged mechanistic studies of the basic function of the machine.

Reduced, simplified ESCRT-III systems have been identified in prokaryotes including in bacteria and archaea (named Vipp1 and PspA in bacteria and CdvB in archaea) (7, 20, 21). While the bacterial homologs were shown to remodel membranes in vitro, no VPS4 was identified in this system so far, and whether these distant homologs can sever membranes has not been clarified. ESCRTs encoded by TACK archaea were shown to participate in cell division, suggesting functional similarities between the eukaryotic and archaeal ESCRT systems (22-25). Within the archaeal domain the Asgard ESCRT system is considerably closer to the eukaryotic system. While all other archaea encode only for homologs of the ESCRT-III/VPS4 module, Asgard archaea encode for

homologs of the complete ESCRT system (ESCRT-I-III and VPS4) (6, 7). Additionally, the sequence of Asgard ESCRT-III/VPS4 proteins is more closely related to those of eukaryotes than to other archaeal ESCRT systems (the CDV system) (5, 20). Lastly, VPS4 homologs of Asgard archaea were shown to functionally interact with eukaryotic ESCRTs in both yeast and mammalian cells (5, 26). Notably, the Asgard ESCRT-III subfamily is substantially reduced compared to eukaryotes with only two ESCRT-III proteins (named here CHMP1-3 and CHMP4-7) encoded in some species including Loki and Heimdall archaeota (1, 5, 7, 26). Hence, the Asgard ESCRT system constitutes a minimalist ESCRT machinery that may hold the core capabilities of eukaryotic ESCRTs and could have been involved in membrane remodelling processes that occurred during eukaryogenesis. Yet, the function, organization, and properties of Asgard ESCRT-III complexes as well as their ability to remodel membranes are mostly unknown.

In this work, we provide the first evidence that Asgard ESCRT-III complexes share functional similarities with eukaryotic ESCRTs. Using purified ESCRT-III homologs encoded by the most abundant Asgard phyla, Lokiarchaeota (Loki), we show that the Asgard ESCRT-III protein CHMP4-7 self-assemble into homo- and hetero- helical tubes that resemble those of eukaryotes (15, 18, 19, 27). The proportion of helical tubes was dramatically enriched in the presence of short DNA oligos, while no filaments could be observed upon DNAse treatment. Notably, Loki ESCRT filaments, formed under any of these conditions, were able to bind and deform small unilamellar vesicles (SUVs) comprised of eukaryotic-like synthetic phospholipids. Hence, Loki ESCRT-III assemble into helical filaments that are affected by oligonucleotides and are capable of remodelling eukaryotic-like membranes.

RESULTS

Eukaryotic ESCRT-III proteins polymerize into helical filaments - a hallmark of ESCRT-III organization that is thought to be essential for their function in membrane remodeling

(8, 28). Polymerization is mediated by the snf7 domain that is conserved in both archaea and eukaryotes, but the polymerization properties of Asgard ESCRT-III has not been examined (5, 20, 26). To investigate the assembly properties of Asgard ESCRT-III proteins, we purified recombinant versions of the ESCRT-III proteins CHMP4-7 and CHMP 1-3, encoded by the Loki GC14_75 strain (KKK44605.1 and KKK42122.1, respectively). Using our assay conditions (see material and methods), full length CHMP 4-7 self-assembled into filaments (Fig 1). No filaments were observed under the same conditions using full length CHMP1-3 (sup Fig. 1A). In negative stain TEM images, CHMP 4-7 was predominantly seen in either long, thin filaments or rod-shaped tubes (Fig 1A, see arrows). A pattern of parallel, periodic stripes was detected in the CHMP 4-7 tube structures by cryo-EM, supporting a helical tube organization (Fig 1B, C). The outer diameter of the CHMP4-7 tubes was variable, ranging between 35 to 55 nm (averaged diameter 44nm ± 30.9). Tube length was typically between 300 - 450 nm (Fig 1D). The overall shape of CHMP4-7 helical tubes resembled the helical tubes previously described for eukaryotic or bacterial ESCRT-III filaments (15, 18, 19, 29). The diameter of Loki CHMP 4-7 helical tubes was slightly larger than the diameters measured for human CHMP1B (~25nm) or the bacterial ESCRT III homologs PspA (~21 nm), but was in the range of diameters measured for human CHMP2A-CHMP3 (38-43 nm) (18, 19, 29). Collectively, these data indicate that Loki CHMP 4-7 spontaneously self-assemble into the typical helical tube organization described for the ESCRT-III complex.

Next, we examined whether, similar to their human homologs, Loki ESCRT-IIIs can assemble into co-polymers (18, 19). To this end, full lengths Loki CHMP4-7 and CHMP 1-3 were incubated at different ratios. While no filaments were seen at 1:1 CHMP4-7-CHMP1-3 ratio, helical tubes could be readily observed at 2:1, 4:1 and 6:1 ratios (Fig 2 and Sup Fig 1B). Notably, CHMP 4-7-CHMP 1-3 helical tubes exhibited different properties than those observed for the CHMP 4-7 homo-polymer. First, their outer diameter was significantly smaller and less diverse (CHMP 4-7-CHMP 1-3 2:1 ratio, 31±7.7) (Fig. 2B, left panel). Second, helical tubes formed in the presence of both CHMP4-7 and CHMP1-3 were significantly longer than those formed by the CHMP4-7 homo-polymer (>X1.5 folds increase for 2:1 and 4:1 ratios) (Fig. 2B, right panel). Third,

the morphology of the CHMP4-7-CHMP1-3 helical tube was slightly different: tubes appeared to be more curved and the periodic stripes, which could only be observed by cryo-EM for CHMP 4-7 homo-polymers, were readily detected in negative stain images of the co-polymer, suggesting that packing of the helical tube is less tight in the presence of CHMP1-3 (Fig 2A). These phenotypic changes were not induced upon substituting CHMP 1-3 with purified GFP, suggesting that they are specifically contributed by CHMP 1-3 (Sup. Fig 1C). We therefore concluded that Loki ESCRT-III proteins assemble into helical tubes composed of homo- and co-polymers with the co-polymers forming longer, narrower, and more homogenous tubes than the homo-polymer. These findings are in line with previous observations obtained for human ESCRT-III CHMP1B homo- and co-polymers (in the presence of IST1), which also formed a narrower, more uniform tubes in the co-polymer composition (30). The realization that both human and Asgard ESCRT-III proteins assemble into homo-and co- polymers with the latter adopting a narrower more uniform tube shape, strongly suggests that this is a basic, conserved property of the ESCRT-III system.

Recent work from our laboratory showed that purified Loki CHMP4-7 binds short DNA oligonucleotides (26). Human CHMP1B, exhibited similar properties and a recently solved cryo-EM structure of human CHMP1B/IST1 filaments demonstrated direct interactions between the ESCRT-III filament and nucleic acids (26, 31). We, therefore, set to examine the effect of short DNA oligonucleotides on the self-assembly properties of Asgard ESCRT-III filaments. A significant increase in helical tube assemblies was observed for the co-polymer in the presence of ssDNA, in both negative stain- and cryo-TEM images (Fig 3A-B and Sup Fig 2A). More helical tubes were also observed upon addition of dsDNA, but to a lower extent. No filaments were observed when incubating CHMP1-3 with DNA, indicating that that observed increase in helical tubes do not result from self-assembly of CHMP1-3 into homo-polymers (Sup Fig. 2D). Addition of ssDNA to CHMP4-7 homo-polymers also led to a dramatic increase in helical tubes, indicating that the effect of DNA is not restricted to the co-polymer (Fig. 3C, Sup Fig 2B). The presence of DNA also affected the properties of the helical tubes. CHMP 4-7-CHMP1-3 helical tubes formed in the presence of either ds- or ss- DNA exhibited larger and more

variable diameters (43.9nm ±58 for CHMP4-7-CHMP1-3 2:1 ssDNA vs CHMP4-7-CHMP1-3 2:1 31nm ±7.7), resembling the diameter measured for the CHMP 4-7 homo-polymer (CHMP4-7 44nm ±30.9) (Fig. 3D). Moreover, filaments were less curved, and the periodic stripes observed in negative stain images in the co-polymer could not be observed (Fig 3A). Addition of DNA did not affect the characteristics length or diameter of tubes formed by CHMP 4-7 homo-polymers (Fig. 3D-E). It, therefore, appears that DNA aids the organization of Loki-ESCRT-III proteins into helical tubes and counteract, at least to some extent, the effect of CHMP1-3 on tube characteristics.

To further investigate the possible effect of DNA on Loki ESCRT-III polymerization, we performed the self-assembly reaction in the presence of DNase. Surprisingly, filament formation was completely abolished for both homo- and co-polymers in the presence of DNase (Fig 3F and Sup Fig. 2E-F). Additionally, no filaments were observed upon incubation with DNAse post self-assembly, suggesting that filament stability and/or integrity are dependent on DNA. Altogether, these findings strongly suggest that DNA is an essential component of Loki ESCRT-III filamentous organization.

Eukaryotic ESCRT-IIIs were shown to bind and deform membranes *in vitro* and in cells (28). To determine whether ESCRTs encoded by Asgard archaea carry the ability to remodel membranes, we incubated Loki ESCRT-III pre-assembled filaments with small unilamellar vesicles (SUVs, ~100 nm) composed of negatively charged eukaryotic-like phospholipids (1:1, PC:PS). Under these conditions, ESCRT-III filaments, assembled under any of the conditions described above (including in the presence of DNA), were found to intimately interact with SUVs (Fig. 4A, B and Sup Fig. 3). We identified four main types of ESCRT-III-SUV interactions: (1) Attachment of the SUV to the outside surface of the tube, which was associated with flattening of the vesicle at the filament-vesicle interface; (2) Docking of the SUV at the tip of the helical tube; (3) Invagination of the SUV to the interior of the ESCRT-III tube; and (4) Dramatic remodeling of both the SUV and the ESCRT-III tube (see examples in Fig. 4C, left panel). Combinations of several types of interactions on the same filament were also observed, indicating that these interactions are not mutually exclusive. Moreover, a docked SUV that invaginates

the helical tube was observed occasionally (Fig. 4B, left panel and sup movies 1, 2), suggesting that these two types of interactions represent successive steps. Invaginations of more than one vesicle to the same tube could be observed, in cryo-TEM and cryo-tomography reconstructions, giving rise to the formation of a complex membrane system with several vesicles internalized into one another (Fig 4B, and sup movies 1, 2). In these complex organizations, which were often accompanied by a considerable deformation of both the filament and the vesicles, the characteristics periodic stripes of the ESCRT-III filament could often be detected at the exterior of the filament-vesicle complex, suggesting that the observed morphologies result from internalization of vesicles into the ESCRT-III helical tube followed by deformation of the tube. Loki ESCRT III filaments also interacted with neutrally charged SUVs (100% PC) but to a much lower extent, exhibiting predominantly binding of the SUV on the outside of the helical tube (Sup Fig. 4). Therefore, Loki ESCRT-III filaments associate with eukaryotic-like membrane vesicles, and deform negatively charged vesicles via the interior of the tube (see proposed model in Fig. 4D).

Last, we asked whether the composition of ESCRT-III helical tubes, described here, affect their capabilities to remodel membranes. Because vesicle-filaments interactions were identified under all conditions, we analyzed the proportion of the four types of filament-vesicle interaction, we identified, in different ESCRT-III compositions. No difference was observed in the distributions of homo- and co- polymers, suggesting that the composition of the filament does not significantly affect membrane indications. The presence of DNA affected the distributions of ESCRT-III-SUV interactions in both the homo- and co- polymers, as follows (Fig. 4C): (1) The association of vesicles with the outside surface of the helical tube was considerably enriched (outside, type 1, No DNA, <15%; with DNA, >35%). (2) Interactions with the tip of the filament (docking, type 2) and invagination of the vesicle (inside, type 3) were significantly enriched. (3) The extent of complete remodeling events (remodeling, type 4) was dramatically reduced (with DNA, ~5%; no DNA ~80%). Therefore, homo- and co- Loki ESCRT-III filaments are capable of interacting and remodeling lipid membranes, both in the presence and

absence of DNA, but the extent of remodeling appear to be attenuated by the presence of DNA.

DISCUSSION

In this work, we provide the first evidence to show that, similar to their eukaryotic homologs, Asgard ESCRT-III proteins assemble into helical filaments that remodel membranes. These findings confirm that ESCRT homologs encoded by Asgard archaea are functionally related to their eukaryotic homologs. We further provide data to support prominent role for DNA in the Asgard ESCRT-III system. Finally, by using SUVs composed of eukaryotic phospholipids, which are fundamentally different from archaeal lipids, we demonstrate that the Asgard ESCRT-III could, in-principle, contribute to the membrane remodeling processes that occurred during eukaryogenesis and gave rise to the complex phospholipids-based endomembrane system of eukaryotes.

Our data point to similarities between the human and Asgard ESCRT-III systems. First, the nature of self-assembly appear to be conserved. Similar to the human CHMP1B-IST1 complex, Loki CHMP4-7 was found to polymerize alone or in the presence of CHMP 1-3, with the homo-polymer exhibiting a wider, more variable diameter compared to the co-polymer (30). What controls the diameter of the ESCRT-III helical tube is currently unknown. Our findings that, similar to their human homologs, Asgard ESCRT-III homo-filaments can adopt a wide range of diameters that can be tuned by the addition of another ESCRT-III components, strongly suggest that this is a conserved feature of the ESCRT-III system. Therefore, a basic feature of the ESCRT-III system may be their ability to assemble into flexible homo filaments that can be tuned to adopt different shapes by incorporating additional ESCRT-III proteins into the polymer. Such a model can explain how the ESCRT-III system execute the large repertoire of membrane remodeling processes in cells, which greatly vary in scales and topologies (7, 8).
The topology of membrane binding, described here for Loki ESCRT-IIIs, resemble the topology reported for the human CHMP1B-IST1 polymer, i.e. bindings via the interior of the helical tube (30). This topology is reversed to the conventional topology attributed to

the ESCRT complex and that was described for the CHMP2A-CHMP3 co-polymer (19, 27), which is binding and deforming membranes via the external surface of the tube. Reversed membrane binding topology was also recently reported for the bacterial ESCRT-III homologs Vipp1 and PspA (29, 32). Whether this topology represent the preferred topology of ancient ESCRTs or is a consequence of the experimental, in vitro, system is yet to be determined. Regardless, these similarities suggest that the ESCRT-III membrane remodeling properties reported here are a common property of the ESCRT system, conserved in all domains of life.

Our results highlight DNA as an essential Loki ESCRT-III partner. Organization of both homo- and co- ESCRT-III polymers into helical tubes was enhanced in the presence of short DNA oligonucleotides and helical tube formation was completely blocked upon addition of DNase. Whether DNA has a role in stabilizing Loki ESCRT-III filaments or in facilitating their nucleation is still unknown. Notably, human CHMP1B-IST1 filaments were shown to bind DNA in the inner side of the tube (31). Additionally, nucleotides were recently resolved in cryo-EM structures of the bacterial ESCRT-III Vipp1 and were suggested to play a role in helical tube stabilization (32). It is therefore tempting to speculate that nucleotide binding is an additional core property of the ESCRT-III machine that is conserved in all domains of life.

Our data show that Loki ESCRT-III filaments that polymerized in the presence of DNA were able to bind and deform membrane vesicles. Yet, the extent of membrane deformation that occurred inside the tube was attenuated, while binding on the exterior of the ESCRT-III tube was enhanced. These results are consistent with competition of DNA and membranes over the same binding sites, located at the interior of the tube, as recently suggested for human CHMP1B (31). Alternatively, the presence of DNA may change the biophysical properties of the tube, thereby resisting the deformation of the tube needed to facilitate membrane remodeling from within. Future experiments allowing direct visualization of ESCRT-III proteins, DNA and the membrane at high resolution are needed in order to examine these models and to resolve the intimate relationship between these three partners.

Overall, the Loki ESCRT-III filaments characterized here, share more similar characteristics to human CHMP1B-IST1 filaments than to human CHMP2A-CHMP3 or yeast snf7 (human CHMP4B) filaments. Filaments of both Asgard ESCRT-III and human CHMP1B, were shown to assemble into homo- and co- polymers with the latter being more constricted; both filaments were reported to bind DNA in vitro; and both deformed membranes via binding to the inner side of the filamentous tube. Consistently, we recently showed that both Loki CHMP4-7 and human CHMP1B associate with chromatin when expressed in mammalian cells (26). We therefore suggest that Asgard ESCRT-IIIs are functionally most similar to CHMP1B in the eukaryotic ESCRT-III system.

The biological function of Asgard ESCRTs has yet to be defined. The findings that Loki ESCRT-III filaments can bind both DNA and membranes raises a few attractive possibilities. First, given the established role of ESCRTs in cell division in TACK archaea and in eukaryotes, it is possible that the ESCRT machinery manifest a basic cell division machinery capable of orchestrating DNA segregation and membrane splitting (22-25). In this regard, the ability of DNA to retain extensive membrane deformation may represent a biological mechanism to avoid premature membrane constriction during cell division. Second, the ESCRT complex may have been involved in nuclear membrane formation during eukaryogenesis, by bringing together membranes and DNA and facilitating DNA encapsulation by membranes. In this respect, mammalian ESCRT-III proteins have been shown to mediate sealing of the nuclear membrane post cell division and to regulate the attachment of heterochromatin to the newly formed nuclear envelop (33-35). Moreover, we recently reported that Loki CHMP 4-7 is targeted to the nucleus when over expressed in eukaryotic cells (26). Finally, the membrane binding experiments performed here were done using eukaryotic-like phospholipids, which are fundamentally different from archaeal lipids but may resemble the lipid composition of the newly formed nuclear membrane. Therefore, the ESCRT-III system encoded by Asgard archaea could have contributed to the

membrane remodeling that occurred during the formation of the phospholipids-based nuclear membrane.

MATERIALS AND METHODS

Cloning

Open reading frames (ORFs) from Loki MAG sp. GC14_75, encoding for CHMP1-3 and CHMP4-7 genes were obtained from NCBI (accession numbers KKK42122.1, KKK44605.1, respectively) were amplified by PCR and sub-cloned into pSH21 vector subsequently to the TEV cleavage tag that followed an N terminal polyhistidine and MBP protein tags (a kind gift from Eyal Gur, BGU, Israel)(36). Plasmids were verified by sequencing.

Protein Expression and Purification

pSH21 plasmids containing Loki CHMP1-3 or CHMP4-7 were expressed Escherichia coli BL21 strain and incubated in LB 50 µg/mL Ampicillin at 37°C until reaching O.D. of 0.6. Then, induction with 0.5 mM IPTG was performed and the cultures were grown at 30°C for 3-4 hours. Cells were then resuspended and lysed by sonication in buffer A (25 mM Hepes pH= 8, 500 mM NaCl, 10% glycerol, 15 mM 2-mercaptoethanol, 10 mM imidazole) supplemented with protease inhibitor cocktail (cOmplete ultra-tablets, EDTA-free, Roche) and 500 µg/ml DNase I (10104159001; Roche Diagnosis GmbH, Manheim, Germany), and the supernatant was clarified by centrifugation (25,000 g, 40 mins, 4°C). For CHMP4-7 purification, supernatant was subjected to HisPur™ Ni-NTA Resin (88222; Thermo Fisher Scientific, Weltham, MA) column and eluted in buffer B (buffer A supplemented with 50 mM imidazole). Protein tags were then removed using a TEV protease (1 mg/10 mg protein) in buffer C (50mM Tris-HCL pH=7.4, 10% glycerol, 500 mM NaCl, 15 mM 2-mercaptoethanol). Finally, a second Ni-NTA step was performed using buffer C and the flow-through was collected.
For CHMP1-3 purification, supernatant was subjected to Ni-NTA column and eluted in buffer B. Samples were then subjected to amylose resin (E8021; NEB, Frankfurt, Germany) in buffer D (20mM Tris pH=7.4, 500 mM NaCl, 10mM β-Mercaptoethanol, 10% Glycerol) and eluted in buffer D supplemented with 10mM maltose. Protein tags

were then removed using a TEV protease (1 mg/10 mg protein) in buffer C (50mM Tris-HCL pH=7.4, 10% glycerol, 500 mM NaCl, 15 mM 2-mercaptoethanol). Finally, a second Ni-NTA step was performed using buffer C and the flow-through was collected. Purified proteins were verified my mass spectrometry.

For polymerization, proteins were incubated in buffer E (25mM Tris pH=7.6, 50 mM KCl) for 5 hours at RT at the indicated conditions. For DNA experiments, ATCCACCTGTACATCAACTCGCCCGGCGGCTCGATCAGCG (40 bases probe), ss or ds were used at the indicted concentrations. DNase I (10104159001; Roche Diagnosis GmbH, Manheim, Germany) was added at 20mg/ml concentrations when indicated.

Preparation of small unilamellar vesicles (SUVs)

Chloroform Lipid solutions (DOPC or DOPS) were purchased from Avanti Polar Lipids Inc. (Albaster, AL, USA catalog number 850375, 840035). Lipid mixtures of DOPC/DOPS 1:1 molar ratio and pure DOPC were prepared at a total concentration of 1 mg/ml in Tris 20 mM, KCl 50 mM, pH 7.8 were prepared. Each lipid suspension was extruded 20 times via a 100 nm polycarbonate membrane using a mini-extruder (Avanti Polar Lipids, Alabaster, AL, USA). In the final stage, the vesicles were mixed with the Asgard Loki ESCRT-III filaments. All experiments were done with 8 μM ESCRT-III and 124 μM vesicles in a buffer of Tris 25 mM, KCl 50 mM, at pH 7.6.

Negative Stain grid preparation and imaging

The negative stain samples for TEM analysis were prepared in the following way: 300 mesh copper grids (Ted Pella, Prod No. 01813-F) were glow discharged to enhance hydrophilicity of their surface. Next, 2.5 uL of the sample was applied on to the grid and the excess liquid was blotted with filter paper after 1 minute. The grid was dried in air for 1 minute, following by applying 5 uL of uranyl acetate 2% solution (SPI CAS# 6159-44-0) for negative staining to increase the sample contrast. Next, the grid was blotted ones more to remove the excess uranyl acetate. Finally, the grid was dried in air before insertion into the microscope. The imaging of the samples was performed with Thermo

Fisher Scientific Talos F200C transmission electron microscope operating at 200 kV. The images were taken with Ceta 16M CMOS camera.

Cryo-electron microscopy

Sample preparation: 3 μL of proteins / proteins-phospholipids mix samples were gently deposited on glow discharged Quantifoil R 1.2/1.3 holey carbon grids (Quantifoil Micro Tools GmbH, Germany). Samples were manually blotted for four seconds at room temperature and vitrified by rapidly plunging into liquid ethane using a home-built plunging apparatus. The frozen samples were stored in liquid nitrogen until imaging.

Micrographs acquisition: Samples were loaded under cryogenic conditions and imaged in low dose mode on a FEI Tecnai F30 Polara microscope (FEI, Eindhoven) operated at 300 kV. Micrographs were collected using SerialEM, at a calibrated pixel size of 1.1 Å by a K2 Summit direct electron detector fitted behind an energy filter (Gatan Quantum GIF) set to ±10 eV around zero-loss peak with total electron dose of 80 ē/Å^2. Each dose-fractionated movie had 50 frames, micrographs sums were aligned in SerialEM.

Cryo-tomography. Micrographs were acquired with a FEI Tecnai F30 Polara microscope (FEI, Eindhoven) operated at 300 kV, using a K2 Summit direct electron detector fitted behind an energy filter (Gatan Quantum GIF), set to ±10 eV slit around the zero-loss peak. Pixel size at the sample plane was 2.3 Å. The camera was operated in counting mode at a dose rate of 6−7 ē/pixels/sec. Tilt series of 41 exposures from −21° to +60° and back to -60° in 3° intervals and a total dose of ~ 120 ē /Å^2 were collected with Serial-EM. Tilt series were aligned, and tomograms were reconstructed using eTomo (IMOD4.11 package) (37). Movies were generated in imageJ.

Measurements and statistical analysis

Filament length and diameter measurements were performed in Velox software version 3.5 (Thermo Fisher Scientific, Inc.).

Statistical analysis was performed in Graph Pad Prism version 9.00 (La Jolla, CA, USA). Unless specified otherwise, comparison between two groups was calculated by

one way ANOVA * p- value ≤ 0.1, **p- value ≤ 0.01, ***p- value ≤ 0.001, ****p-value ≤ 0.0001.

ACKNOWLEDMENTS

We thank the laboratories of Eyal Gur (BGU) and Eyal Arbely (BGU) for their practical advice on proteins expression and purifications and for kindly sharing their reagents and equipment with us. We also thank Itzik Mizrahi (BGU) and Ori Avinoam (WIS) for constructive feedback on the project. Last, we thank all members of the Elia lab for critical feedback throughout the project. The Elia laboratory is funded by the Israeli Science Foundation (ISF) Grant no. 1323/18. ABG is grateful to the Israel Science Foundation for financial support (grant 2101/20).

AUTHOR CONTRIBUTIONS

NE and DN conceptualized the project. NM performed and analyzed all experiments. GH and AB, were in charge of experiments using SUVs. AU acquired negative stain TEM images. RZ acquired and analyzed cryo-EM data. NE, DN, AB and RZ were involved in experimental design and data analysis. NE wrote the manuscript. All authors read and revised the manuscript.

Competing Interest Statement: We declare no competing interest

REFERENCES

1. K. Zaremba-Niedzwiedzka *et al.*, Asgard archaea illuminate the origin of eukaryotic cellular complexity. *Nature* **541**, 353-358 (2017).
2. F. MacLeod, G. S. Kindler, H. L. Wong, R. Chen, B. P. Burns, Asgard archaea: Diversity, function, and evolutionary implications in a range of microbiomes. *AIMS Microbiol* **5**, 48-61 (2019).
3. A. Spang *et al.*, Complex archaea that bridge the gap between prokaryotes and eukaryotes. *Nature* **521**, 173-179 (2015).
4. E. Neveu, D. Khalifeh, N. Salamin, D. Fasshauer, Prototypic SNARE Proteins Are Encoded in the Genomes of Heimdallarchaeota, Potentially Bridging the Gap between the Prokaryotes and Eukaryotes. *Curr Biol* **30**, 2468-2480 e2465 (2020).
5. Z. Lu *et al.*, Coevolution of Eukaryote-like Vps4 and ESCRT-III Subunits in the Asgard Archaea. *mBio* **11** (2020).
6. T. Hatano *et al.*, Asgard archaea shed light on the evolutionary origins of the eukaryotic ubiquitin-ESCRT machinery. *Nat Commun* **13**, 3398 (2022).
7. Y. Caspi, C. Dekker, Dividing the Archaeal Way: The Ancient Cdv Cell-Division Machinery. *Front Microbiol* **9**, 174 (2018).
8. J. H. Hurley, ESCRTs are everywhere. *EMBO J* **34**, 2398-2407 (2015).
9. Y. A. M. Alonso, S. M. Migliano, D. Teis, ESCRT-III and Vps4: a dynamic multipurpose tool for membrane budding and scission. *FEBS J* **283**, 3288-3302 (2016).
10. J. McCullough, L. A. Colf, W. I. Sundquist, Membrane fission reactions of the mammalian ESCRT pathway. *Annu Rev Biochem* **82**, 663-692 (2013).
11. C. Caillat, S. Maity, N. Miguet, W. H. Roos, W. Weissenhorn, The role of VPS4 in ESCRT-III polymer remodeling. *Biochem Soc Trans* **47**, 441-448 (2019).
12. S. Maity *et al.*, VPS4 triggers constriction and cleavage of ESCRT-III helical filaments. *Sci Adv* **5**, eaau7198 (2019).
13. B. E. Mierzwa *et al.*, Dynamic subunit turnover in ESCRT-III assemblies is regulated by Vps4 to mediate membrane remodelling during cytokinesis. *Nat Cell Biol* **19**, 787-798 (2017).
14. A. K. Pfitzner *et al.*, An ESCRT-III Polymerization Sequence Drives Membrane Deformation and Fission. *Cell* **182**, 1140-1155 e1118 (2020).
15. W. M. Henne, N. J. Buchkovich, Y. Zhao, S. D. Emr, The endosomal sorting complex ESCRT-II mediates the assembly and architecture of ESCRT-III helices. *Cell* **151**, 356-371 (2012).
16. I. Goliand *et al.*, Resolving ESCRT-III Spirals at the Intercellular Bridge of Dividing Cells Using 3D STORM. *Cell Rep* **24**, 1756-1764 (2018).
17. J. Guizetti *et al.*, Cortical constriction during abscission involves helices of ESCRT-III-dependent filaments. *Science* **331**, 1616-1620 (2011).
18. J. McCullough *et al.*, Structure and membrane remodeling activity of ESCRT-III helical polymers. *Science* **350**, 1548-1551 (2015).
19. S. Lata *et al.*, Helical structures of ESCRT-III are disassembled by VPS4. *Science* **321**, 1354-1357 (2008).
20. B. P. Frohn, T. Hartel, J. Cox, P. Schwille, Tracing back variations in archaeal ESCRT-based cell division to protein domain architectures. *PLoS One* **17**, e0266395 (2022).

21. J. Liu *et al.*, Bacterial Vipp1 and PspA are members of the ancient ESCRT-III membrane-remodeling superfamily. *Cell* **184**, 3660-3673 e3618 (2021).
22. A. C. Lindas, E. A. Karlsson, M. T. Lindgren, T. J. Ettema, R. Bernander, A unique cell division machinery in the Archaea. *Proc Natl Acad Sci U S A* **105**, 18942-18946 (2008).
23. R. Y. Samson, T. Obita, S. M. Freund, R. L. Williams, S. D. Bell, A role for the ESCRT system in cell division in archaea. *Science* **322**, 1710-1713 (2008).
24. R. Y. Samson *et al.*, Molecular and structural basis of ESCRT-III recruitment to membranes during archaeal cell division. *Mol Cell* **41**, 186-196 (2011).
25. G. Tarrason Risa *et al.*, The proteasome controls ESCRT-III-mediated cell division in an archaeon. *Science* **369** (2020).
26. D. Nachmias *et al.* (2022) Asgard ESCRT-III and VPS4 reveal evolutionary conserved chromatin binding properties of the ESCRT machinery. in *bioRxiv*
27. K. Azad *et al.* (2022) Structural basis of CHMP2A-CHMP3 ESCRT-III polymer assembly and membrane cleavage. in *bioRxiv*.
28. Y. Olmos, The ESCRT Machinery: Remodeling, Repairing, and Sealing Membranes. *Membranes (Basel)* **12** (2022).
29. B. Junglas *et al.*, PspA adopts an ESCRT-III-like fold and remodels bacterial membranes. *Cell* **184**, 3674-3688 e3618 (2021).
30. H. C. Nguyen *et al.*, Membrane constriction and thinning by sequential ESCRT-III polymerization. *Nat Struct Mol Biol* **27**, 392-399 (2020).
31. N. Talledge *et al.* (2018) The ESCRT-III proteins IST1 and CHMP1B assemble around nucleic acids. in *bioRxiv*.
32. T. K. Gupta *et al.*, Structural basis for VIPP1 oligomerization and maintenance of thylakoid membrane integrity. *Cell* **184**, 3643-3659 e3623 (2021).
33. G. H. Pieper, S. Sprenger, D. Teis, S. Oliferenko, ESCRT-III/Vps4 Controls Heterochromatin-Nuclear Envelope Attachments. *Dev Cell* **53**, 27-41 e26 (2020).
34. Y. Olmos, L. Hodgson, J. Mantell, P. Verkade, J. G. Carlton, ESCRT-III controls nuclear envelope reformation. *Nature* **522**, 236-239 (2015).
35. M. Vietri *et al.*, Spastin and ESCRT-III coordinate mitotic spindle disassembly and nuclear envelope sealing. *Nature* **522**, 231-235 (2015).
36. Y. Elharar *et al.*, Survival of mycobacteria depends on proteasome-mediated amino acid recycling under nutrient limitation. *EMBO J* **33**, 1802-1814 (2014).
37. D. N. Mastronarde, Automated electron microscope tomography using robust prediction of specimen movements. *J Struct Biol* **152**, 36-51 (2005).

FIGURES AND FIGURES LEGENDS

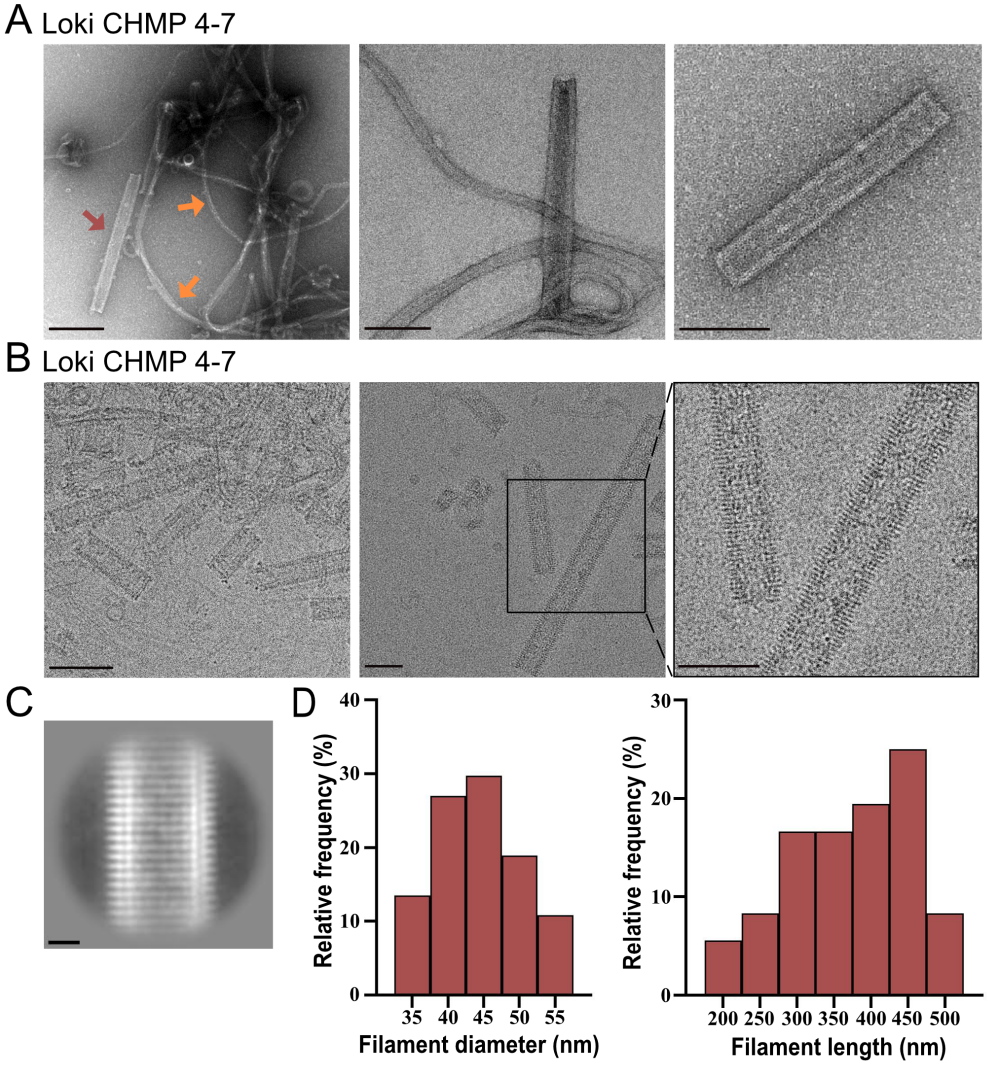

Fig 1. Loki CHMP4-7 protein self-assemble into filaments and helical tubes. **A.** Negative- stain TEM micrographs of Loki CHMP4-7 homo-filaments. Representative zoomed-out (left, scale = 200 nm) and zoomed- in (middle and right, scale = 100 nm) images are shown. Orange arrows indicate filaments, red arrow indicates a helical tube. **B.** Representative Cryo-EM micrographs of Loki CHMP4-7 homo-polymers. Left, zoomed-out image (Scale = 100 nm), middle and right, zoomed-in images (Scale = 50 nm). Box in middle panel specify the zoomed-in region shown to the right. **C.** A representative 2D class average of 502 particles extracted from CHMP 4-7 projections. Scale = 100 Å. **D.** Measurements of Loki CHMP4-7 helical diameters (left, n = 37) and

length (right, n = 36) obtained from negative stain TEM images acquired from two independent experiments. Averaged CHMP 4-7 helical tube diameter 44nm±30.9.

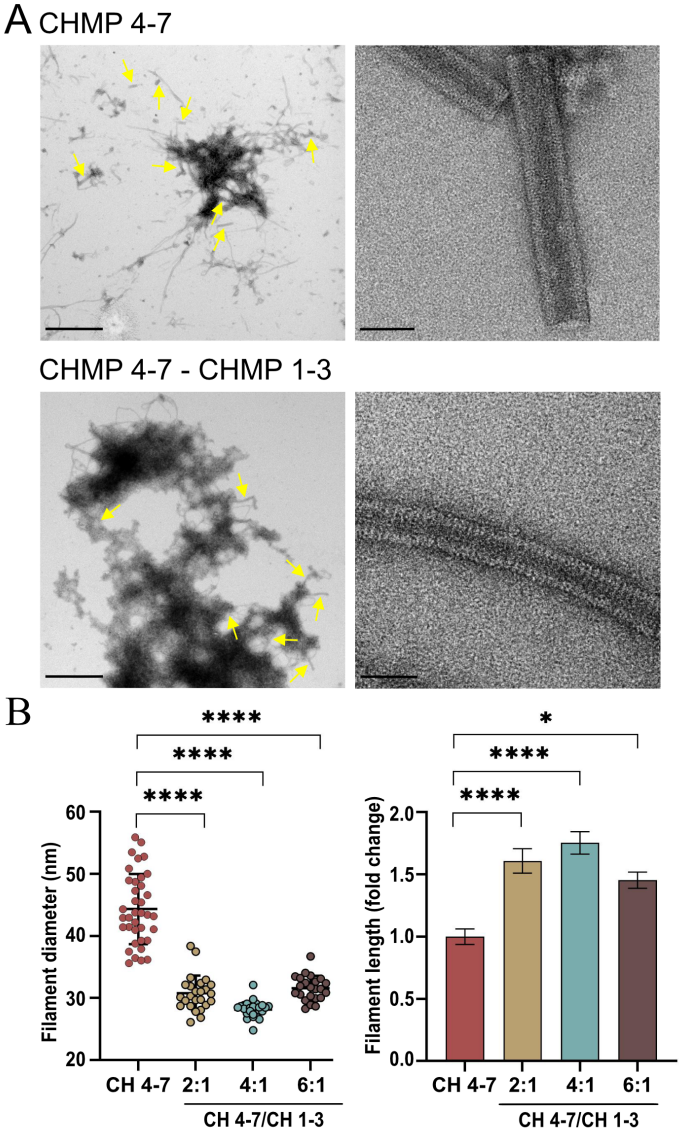

Fig 2. Loki CHMP4-7 and CHMP1-3 co-polymers assemble into helical tubes exhibiting different properties from CHMP 4-7 homo-polymers.

A. Representative Negative- stain TEM images of Loki CHMP4-7 homo-polymers (upper panels) and CHMP4-7-CHMP1-3 co-polymers (bottom panels, 2:1 molar ratio). Zoomed- out (left, scale = 1 μm) and zoomed- in (right, scale = 50 nm) images are shown. Yellow asterisks indicate helical tubes. **B**. Measurements of CHMP4-7-CHMP1-3 hetero-filaments diameters (left) and length (right) at the indicated molar ratios obtained from negative stain TEM images. Averaged diameters (nm): 2:1 ratio, 31±7.7; 4:1 ratio 28±1.6, 6:1 ratio 32±3.8. n = 25 for each condition.

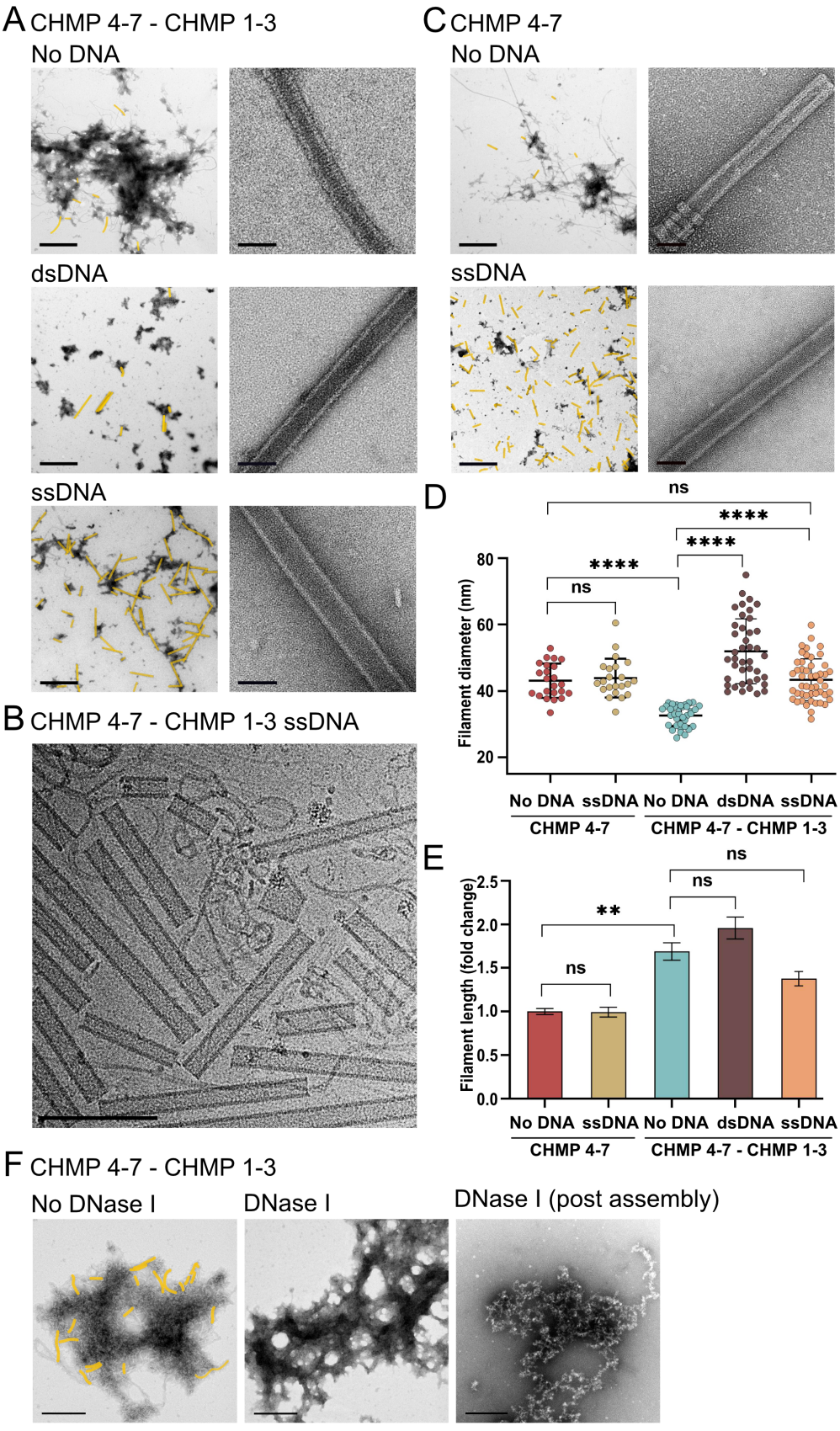

596

Fig 3. Organization into helical tubes is increased in the presence of DNA

A. Negative- stain TEM micrographs of CHMP 4-7-CHMP 1-3 co- polymers (2:1 molar ratio) in the presence of 4.6 μM 40 bases oligonucleotides (ssDNA or dsDNA, as indicated). Representative zoomed- out (left, Scale = 1 μm) and zoomed- in (right, Scale = 50 nm) images are shown. Helical tubes are colored in yellow in zoomed out images to highlight the observed increase in tubes (raw images are provided in Sup Fig 2A). **B**. Representative Cryo-EM images of CHMP 4-7– CHMP 1-3 co-polymers (molar ratio, 4:1) in the presence of ssDNA. Scale = 200 nm. **C.** Negative- stain TEM micrographs of CHMP 4-7 homo-polymers in the presence of 4.6 μM 40 bases ssDNA. Representative zoomed- out (left, Scale = 1 μm) and zoomed- in (right, Scale = 50 nm) images are shown. Helical tubes are colored in yellow in zoomed out images to highlight the observed increase in tubes (raw images are provided in Sup Fig 2B). **D-E** Diameter (**D**) and length (**E**) measurements of helical tubes formed by homo- and the co-polymers (2:1 ratio) in the presence of nucleic acids obtained from negative stain TEM images. Averaged diameters (nm): CHMP4-7 ssDNA 43.9±33, n=21; CHMP4-7-CHMP1-3 2:1 dsDNA 51.9±94, n=44; CHMP4-7-CHMP1-3 2:1 ssDNA 43.9±58, n=48). **F**. Representative Negative- stain TEM images of co-polymers (molar ratio 2:1) upon addition of 20 mg/ml DNase I during (middle panel) or after (right panel) polymerization. Helical tubes are colored in yellow. Scale =200 nm. Data was reproduced in four independent experiments.

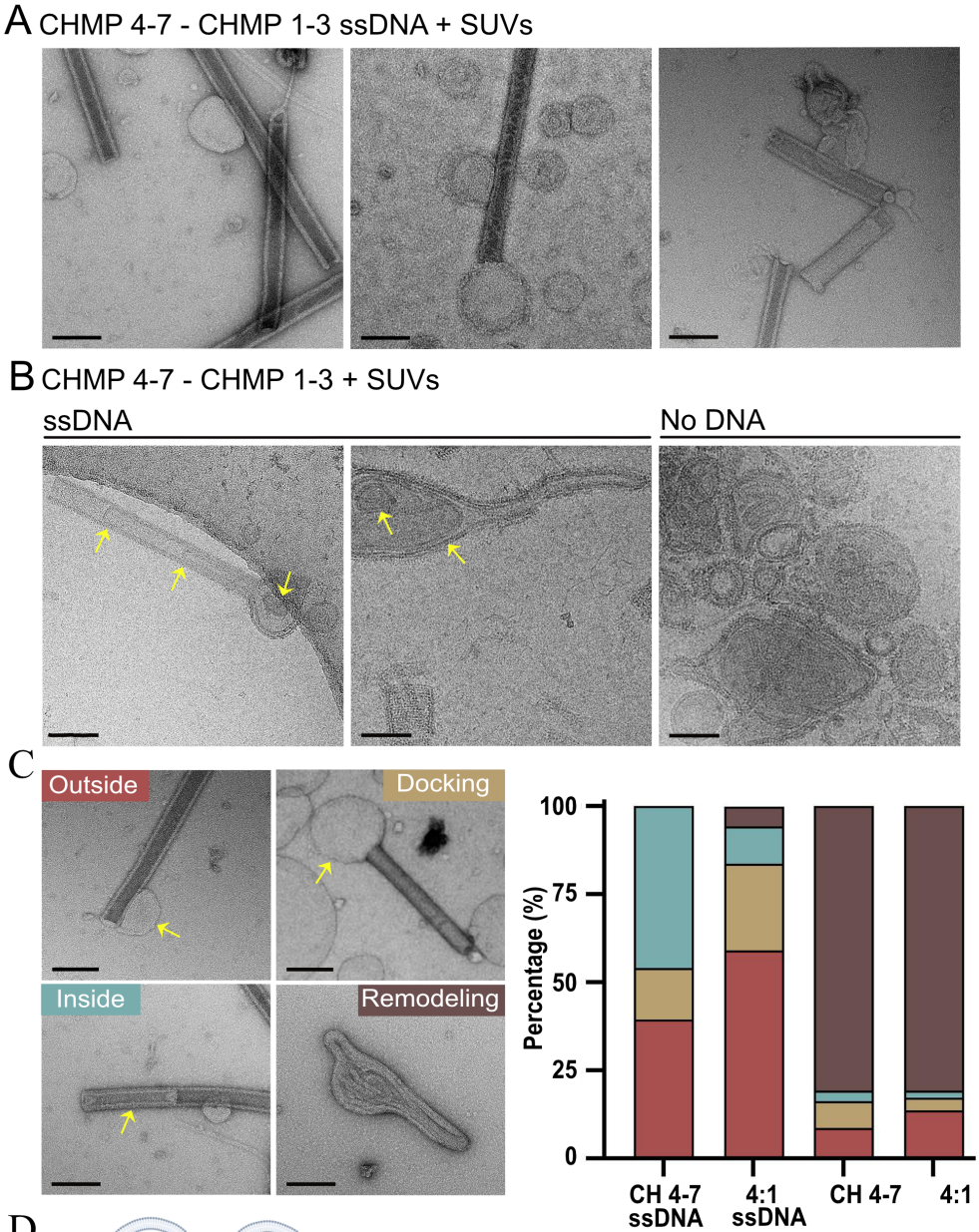

628

Fig 4. Loki ESCRT-III filaments induce membrane remodeling

A-B. Representative Negative- stain TEM (**A**) and Cryo-EM images (**B**) of CHMP4-7-CHMP1-3 (molar ratio, 4:1) polymerized in the presence of ssDNA (10 μM) and incubated with SUVs (DOPC:DOPS, 1:1 ratio). Scale = 100 nm. Arrows in **B** specify internalized vesicles. Reconstructed tomograms of filaments collected from the same grid are provided in Sup. movies 1 and 2. **C**. Percentages of the different types of vesicle-tube interactions observed under the specified conditions. Left panel, represented negative-stain images of the four types of interactions quantified. Outside, attachment of SUV to the outside of the helical tube (type 1); Docking, binding of the vesicle to the tip of the helical tube (type 2); Inside, invagination of the SUV to the helical tube (type 3); Remodeling, deformation of both the vesicles and the ESCRT-III helical tube (type 4). Data was quantified from negative stain imaged obtained in 3 independent experiments (n = CHMP4-7 ssDNA, 124; CHMP4-7-CHMP1-3 ssDNA, 159; CHMP4-7, 197; CHMP4-7-CHMP1-3, 161). Scale = 100 nm. Chi square statistical analysis show a significant difference in the distributions of CHMP4-7 ssDNA vs CHMP4-7 (****p- value ≤ 0.0001), CHMP4-7-CHMP1-3 ssDNA vs CHMP4-7-CHMP1-3 (****p- value ≤ 0.0001), and CHMP4-7 ssDNA vs CHMP4-7-CHMP1-3 ssDNA (****p-value ≤ 0.0001). No significance was found in the distributions of CHMP4-7 vs CHMP4-7-CHMP1-3. **D**. A suggested model for Loki ESCRT-III mediated vesicle remodeling. Vesicles dock at the tip of the ESCRT-III tube. Docking allows the vesicle to directly interact with the interior of the tube, leading to deformation and invagination of the vesicle by the ESCRT-III filament. This process occurs repeatedly leading to the formation of a complex membrane network inside the helical tube, which pushes the ESCRT-III tube from the inside and ultimately causing deformation and remodeling of the tube. This stage is inhibited in the presence of DNA, resulting the accumulation of ESCRT-III-SUV interactions in all the stages that preceded this complete remodeling stage.